Journal of Applied Physics ARTICLE scitation.org/journal/jap

Highly ordered graphite (HOPG) to hexagonal diamond (lonsdaleite) phase transition observed on picosecond time scales using ultrafast x-ray diffraction

Cite as: J. Appl. Phys. **132**, 055901 (2022); doi: 10.1063/5.0085297
Submitted: 14 January 2022 · Accepted: 18 June 2022 ·
Published Online: 1 August 2022

View Online Export Citation CrossMark

Michael R. Armstrong,[1,a)] Harry B. Radousky,[1,a)] Ryan A. Austin,[1] Oliver Tschauner,[2,a)] Shaughnessy Brown,[3] Arianna E. Gleason,[3] Nir Goldman,[1] Eduardo Granados,[3] Paulius Grivickas,[1] Nicholas Holtgrewe,[5] Matthew P. Kroonblawd,[1] Hae Ja Lee,[3] Sergey Lobanov,[6] Bob Nagler,[3] Inhyuk Nam,[3] Vitali Prakapenka,[7] Clemens Prescher,[8] Evan J. Reed,[4] Elissaios Stavrou,[1] Peter Walter,[3] Alexander F. Goncharov,[5] and Jonathan L. Belof[1]

AFFILIATIONS

[1]Department of Physical and Life Sciences, Lawrence Livermore National Laboratory, Livermore, California 94551, USA
[2]Department of Geoscience, UNLV, Las Vegas, Nevada 89154-4010, USA
[3]Matter in Extreme Conditions, SLAC National Accelerator Laboratory, Menlo Park, California 94025, USA
[4]Department of Materials Science and Engineering, Stanford University, Stanford, California 94305, USA
[5]Earth and Planets Laboratory, Carnegie Institution for Science, Washington, DC 20015, USA
[6]Institut für Geowissenschaften, Universität Potsdam, Golm, Germany
[7]GSECARS, Argonne National Laboratory, Argonne, Illinois 60439, USA
[8]Institute of Earth and Environmental Science, University of Freiburg, Freiburg, Germany

14 December 2023 08:14:40

Note: This paper is part of the Special Topic on Shock Behavior of Materials.

[a)]**Authors to whom correspondence should be addressed:** armstrong30@llnl.gov; radousky1@llnl.gov; and oliver.tschauner@unlv.edu

ABSTRACT

The response of rapidly compressed highly oriented pyrolytic graphite (HOPG) normal to its basal plane was investigated at a pressure of ~80 GPa. Ultrafast x-ray diffraction using ~100 fs pulses at the Materials Under Extreme Conditions sector of the Linac Coherent Light Source was used to probe the changes in crystal structure resulting from picosecond timescale compression at laser drive energies ranging from 2.5 to 250 mJ. A phase transformation from HOPG to a highly textured hexagonal diamond structure is observed at the highest energy, followed by relaxation to a still highly oriented, but distorted graphite structure following release. We observe the formation of a highly oriented lonsdaleite within 20 ps, subsequent to compression. This suggests that a diffusionless martensitic mechanism may play a fundamental role in phase transition, as speculated in an early work on this system, and more recent static studies of diamonds formed in impact events.

Published by AIP Publishing. https://doi.org/10.1063/5.0085297

I. INTRODUCTION

The graphite–diamond phase transition (phase diagram shown in Fig. 1) is of particular interest for fundamental reasons[1] and a wide range of applications.[2–5] At static pressure and temperature, graphite transforms into diamond along a positive Clapeyron slope above 1.94 GPa at 0 K to 5.5 GPa at 1700 K.[6,7] On very fast compression time scales, material kinetics hinders the transition to an equilibrium cubic diamond crystal structure. Shock wave compression of graphite typically requires pressures above 50 GPa to observe the phase transition on the time scale of shock compression

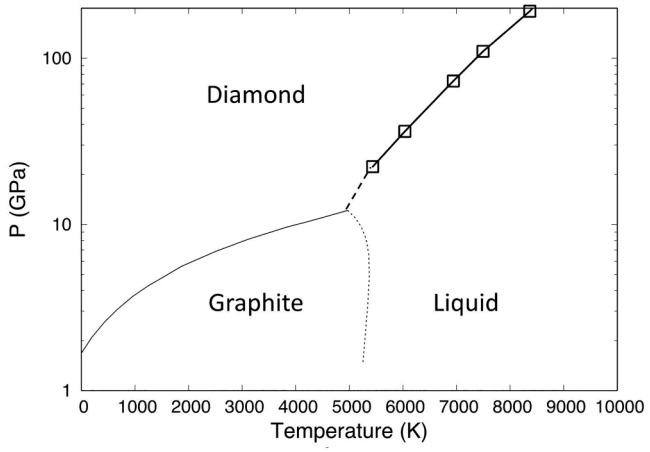


FIG. 1. HOPG phase diagram. Open squares are from *ab initio* calculations.[7]

experiments.[8–11] Furthermore, a hexagonal polytype of diamond (lonsdaleite, diamond-2H) has been observed in shock-compressed material subsequent to impact events,[12] suggesting that the time scale of compression plays a strong role in the phase transition.

The observation of lonsdaleite under shock compression has been a persistent mystery, including the debate over whether hexagonal diamond actually exists, or is an equilibrium cubic diamond rich in aperiodic stacking faults.[13] Previous studies of the phase transition of graphite to diamond or lonsdaleite under moderate shock compression[8,14,15] support a martensitic mechanism for the phase transition, but these studies did not observe atomic structure, so the transformation mechanism was not revealed. More recent studies of impact-formed diamond support the shock formation hypothesis via the observation of large, strongly textured crystals,[16] and rapid out-of-plane (non-diffusional) boat and chair type distortions.[17] Diffraction-based studies of shockwave compressed carbon typically observe lonsdaleite on greater than nanosecond time scales subsequent to compression. In these experiments, we have used the unique capability of MEC/LCLS to explore the phase transition behavior of carbon subsequent to picosecond scale compression shock rise times followed by ~100 ps sustained compression. At comparable time scales, advanced ultrafast experiments have observed fundamental aspects of material behavior under rapid compression, including plasticity,[18–22] chemistry,[23,24] phase transitions,[9,14] and small scale, extreme compression.[25,26] Generally, ultrafast compression experiments have been used to investigate the previously unknown states of matter under extreme elastic compression,[18,19,27] sub-100 ps martensitic phase transitions,[28] and strain rate dependent shock-induced chemistry,[23,29,30] but the response of graphite to ultrafast compression has not previously been investigated on picosecond time scales.

Simulations[31] suggest that an ultrafast, non-equilibrium transformation between highly ordered graphite and diamond may occur with a very strong (>100 GPa), fast (<1 ps) compression wave applied normally to the basal plane of the graphite. The transformation mechanism for this scheme is thought to differ from the conventional near-equilibrium mechanism. In particular, the ultrafast mechanism is predicted to involve a transient "layered diamond" intermediate state,[31] which is not thought to be involved in the near-equilibrium phase transition. Previous experimental works[8,14] employed conventional velocimetry and thermodynamic calculations based on extrapolations. Erskine and Nellis[8] concluded that the transformation mechanism was martensitic (not diffusive) but did not observe atomic structure. In general, works involving ultrafast laser pulses[32–34] have not applied *in situ* characterization of the atomic structure through transformation. In this work, MEC provides a unique opportunity to characterize an atomic structure with picosecond time resolution.

II. EXPERIMENTAL DESCRIPTION

A schematic of the experiment is shown in Fig. 2. The samples comprise a 1 or 2 μm (depending on the sample used for a given energy) Al front surface ablator coating <10 μm thick HOPG samples on a 500 μm thick ~2.5 cm diameter Si wafer with a 15 × 15 matrix of chemically etched wells, through which the sample is laser-shocked in a given shot (similar to the sample configuration for previous experiments on Zr[35,36]). Using this configuration, we can obtain hundreds of shots per wafer. The rear of the sample is coated with a ~50 nm Al layer. The ablator is driven by a ~120 ps full-width half maximum (FWHM) duration laser pulse with <30 μm spot size, and a fast (sub-20 ps, consistent with previous work—see Armstrong *et al.*[35] and Radousky *et al.*[36]) initial rise launching a shock wave of similar duration into the ablator. The x-ray diffraction experiment is comparable to previous works,[35–37] where the shock wave transits the ablator and enters the HOPG sample, and rapid compression initiates a compression-driven structural change. After a variable delay, a ~100 fs duration, 1.301 Å wavelength x-ray pulse is used to obtain an x-ray

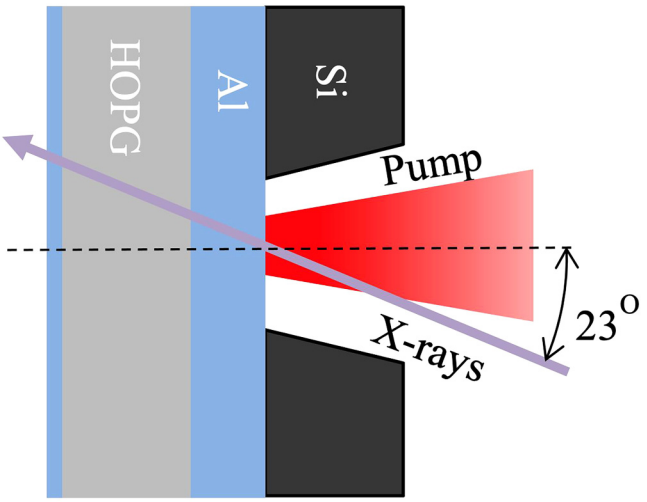


FIG. 2. A schematic of ultrafast laser-driven shock compression experiments on HOPG with XRD at LCLS. Here, Al coated both sides of the sample with a 1–2 μm thick layer on the drive side and a thin layer on the opposite side.

14 December 2023 08:14:40

diffraction (XRD) pattern from the sample, providing structural information during compression wave transit through the sample. Diffraction patterns were collected using three CSPAD detectors, each collecting a single frame per shot. Using this method, the progress of structural transformations in the HOPG sample can be tracked with picosecond time resolution. The laser arrival time at the ablator is determined by observation of the delay time at which shifted Al ablator peaks are observed in lower energy shots—the accuracy of this estimate is within ~20 ps. The peak pressures in these experiments were determined from Zr experiments at the same drive and sample conditions for the Al ablator;[35,36] the HOPG samples were obtained commercially from Optigraph[38] with thicknesses of 5–7 μm. Pre-shot data showed that the samples were very strongly oriented in the 001 direction for hexagonal graphite; except for the 002 reflection, no other diffraction signal was observed prior to the shock experiment, consistent with a very strong orientation along the 001 direction. Calibration of sample–detector distance and geometric correction was conducted with Dioptas.[39] Parasitic scattering, likely due to a misaligned pinhole and noticeable as an intense off-center diffraction artifact (see below), was observed but did not significantly impact the analysis. A slightly different background level of the different detector segments generates artifactual features in the integrated diffraction patterns and requires a further restriction of the regions of integration. After the integration with Dioptas, the sample zero-offset was checked and corrected by using the diffraction signal of unstressed aluminum at the rear of the sample.

Diffraction patterns integrated over the entire azimuthal range were analyzed with Powder Cell[40] by modeling and refining diffraction patterns of the unshocked Al from the rear coating, shock-compressed Al, and the features of the carbon phases. PseudoVoigt profiles with fixed mixing terms and refined Gaussian terms were used in modeling the patterns. The background was fitted with fourth order polynomials. Diffraction features of highly oriented phases (see Fig. S1 in the supplementary material) were fitted with the LeBail approach, whereas smooth extended Debye fringes were fitted with the Rietveld approach. The smooth extended Debye fringes of shocked and unshocked Al were fitted with the Rietveld approach. Diffraction features of the highly oriented carbon phases (Fig. S1 in the supplementary material) were also initially modeled with the Rietveld approach and the preferred orientation was fitted with the March–Dollase approach. However, since the orientation of carbon phases was generally along more than one axis, and because only one or two orientation axes could be fitted, the observed intensities could not be fully modeled in all cases and a LeBail fit was conducted as a final step to show at least the peak profile fit of modeled and observed diffraction features without weighting their structure factors. Details of these fits are described in the supplementary material. Separately, the diffraction patterns were also integrated over smaller regions where shock compression-induced peaks appeared, and peak positions were analyzed as shown below. Both analyses are consistent with the formation of lonsdaleite at early times during compression and reversion to the graphite phase, subsequent to the release of pressure.

III. EXPERIMENTAL RESULTS

Shock compression data were taken at laser drive energies ranging from 2.5 to 250 mJ. This resulted in peak pressures ranging from 10 to 100 GPa in the Al ablator, determined by estimates of the peak shock-induced strain in the sample combined with hydrodynamics simulations employing the known equation of state of aluminum.[35,36] Intermediate pressures were obtained, but did not yield any obvious evidence for diamond phases at pressures (in the Al) less than 100 GPa, for shots up to pressures of ~40 GPa in the ablator. Peak pressures for the Al ablator are consistent with previously published Al/Zr data[35,36] and impedance matching to the known Hugoniot of graphite gives pressures in HOPG around 80% of the pressure in Al. In particular, the difference of 100× in laser intensity (between the 2.5 and 250 mJ drive energies) gave a difference of 10× in the shock drive pressure, as expected from the square root dependence of pressure on laser intensity, i.e., $P \propto I^{0.5}$.[41]

Hydrodynamic simulations[35,36] of shock wave propagation through the samples are shown in Fig. 3 for 2.5 and 250 mJ drive energies. These simulations are calibrated by empirical estimates of pressure from diffraction data in Radousky *et al.*[36] and Armstrong *et al.*[35] and are employed principally to corroborate the shock arrival time at the Al/HOPG interface with shock-induced changes in the HOPG diffraction pattern. From the positions of ambient Al x-ray peaks subsequent to the arrival of the laser drive, but prior to the arrival of the shock wave, preheating of the sample is estimated to be negligible.[35] The simulations utilize a pressure drive that has been calibrated to reproduce the shocks generated by laser ablation on the LCLS platform. Here, we account for an ablated material at the drive surface, as determined from previous works on Al ablators at the same drive conditions.[36] The simulations are adiabatic with an initial mesh size of 5 nm and a time step determined by the Courant condition. The mechanical response of the Al layers is described using a Grüneisen equation of state (EOS).[42] For the HOPG layers, we initially utilized a Grüneisen EOS for graphite[42] but this model was found to be mechanically unstable at larger compressions (relative volumes of less than ~0.6). Therefore, we re-parameterized HOPG EOS using the gas-gun Hugoniot data for graphite[43] and more recent data that achieved higher pressures (up to ~200 GPa), using laser-driven compression experiments.[10] Although the HOPG EOS does not explicitly account for phase transitions, it captures the bulk compressibility with sufficient accuracy for our purposes (identification of wave arrival times, compression duration, etc.). The details of EOS parameterization and fitting results are given in the supplementary material.

From the hydrodynamic simulations, we obtain predictions of shock arrival at the HOPG layer that is accurate to within 20 ps, as confirmed by the appearance of lonsdaleite peaks in the x-ray diffraction data. As shown in Fig. 3, we estimate the thickness of compressed HOPG over the compression time (i.e., for the 2D diffraction patterns shown in Figs. 4 and 5) is less than 500 nm. As shown in Fig. 4, highly textured, spotty diffraction peaks consistent with lonsdaleite appear within approximately 20 ps, subsequent to shock arrival in the HOPG sample. Al diffraction lines are polycrystalline rings spanning the entire azimuthal range. All 250 mJ shots at delays within the compression time of HOPG exhibited the appearance of a similar diffraction signal subsequent to compression. Both shocked and unshocked Al generated smooth Debye fringes. In the 250 mJ runs, shocked Al exhibited very broad diffraction features and additional scattering at diffraction angles

14 December 2023 08:14:40

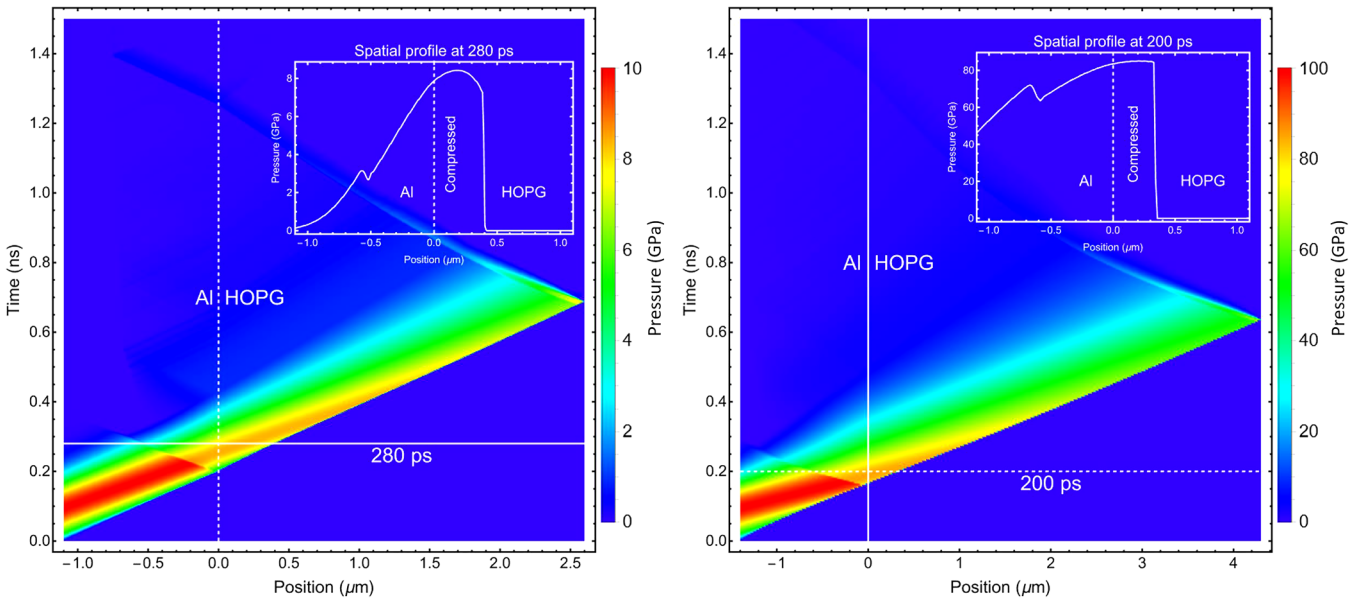


FIG. 3. Hydrodynamic simulations of HOPG compression for drive energies of 2.5 (left) and 250 mJ (right). Pressure is plotted in the Lagrangian space-time plane. The estimates of pressure in aluminum are consistent with previous works on Zr.[35,36] The insets show the pressure profile at 280 ps (2.5 mJ) and 200 ps (250 mJ) subsequent to compression wave arrival in HOPG. Note that different energies involve different initial thicknesses of HOPG.

where Bragg diffraction is extinct in the regular Al fcc lattice. This is consistent with the melting of Al.

Figure 5 shows the 2D diffraction patterns over windows around peaks that appear subsequent to compression at 160 ps delay (just subsequent to HOPG compression) with corresponding integrated patterns. While under compression, we consistently observe the transformation from HOPG to lonsdaleite in all ~100 GPa (in Al) compressed data as early as 160 ps subsequent to shock launch into the Al ablator (i.e., just subsequent to the shock compression of HOPG—see Fig. 3, right side). Lonsdaleite is

14 December 2023 08:14:40

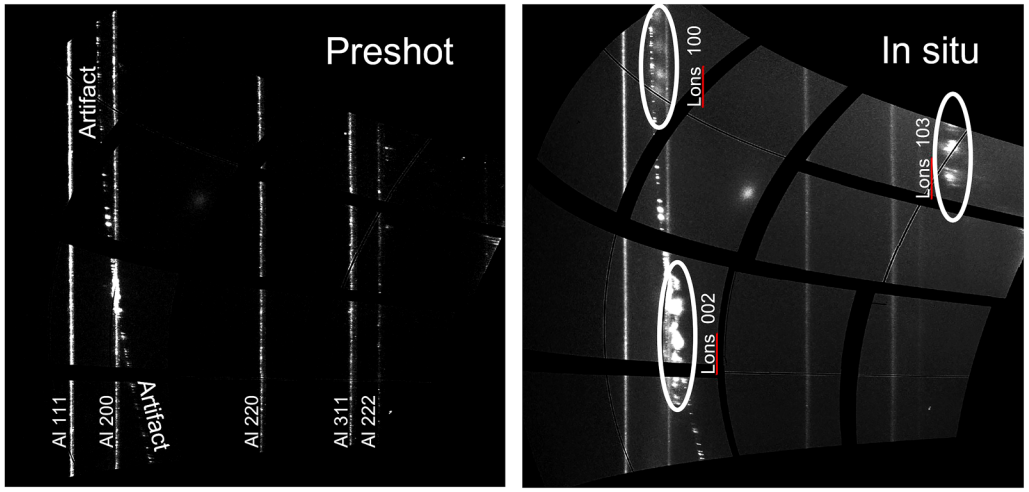


FIG. 4. Pre-shot and *in situ* cake diffraction data for a shot at 160 ps time delay, 250 mJ drive energy. The diffraction angle is along the horizontal axis, increasing to the right, and the azimuthal axis is vertical. A curved artifact in the data (labeled in the pre-shot image) is likely due to a misaligned pinhole. Unlike shock modulated signal from HOPG or Al, the spot pattern for the artifact did not change between pre-shot and *in situ* images. Solid Al lines in the *in situ* data are due to the thin (unshocked, solid) layer of Al on the rear of the sample.

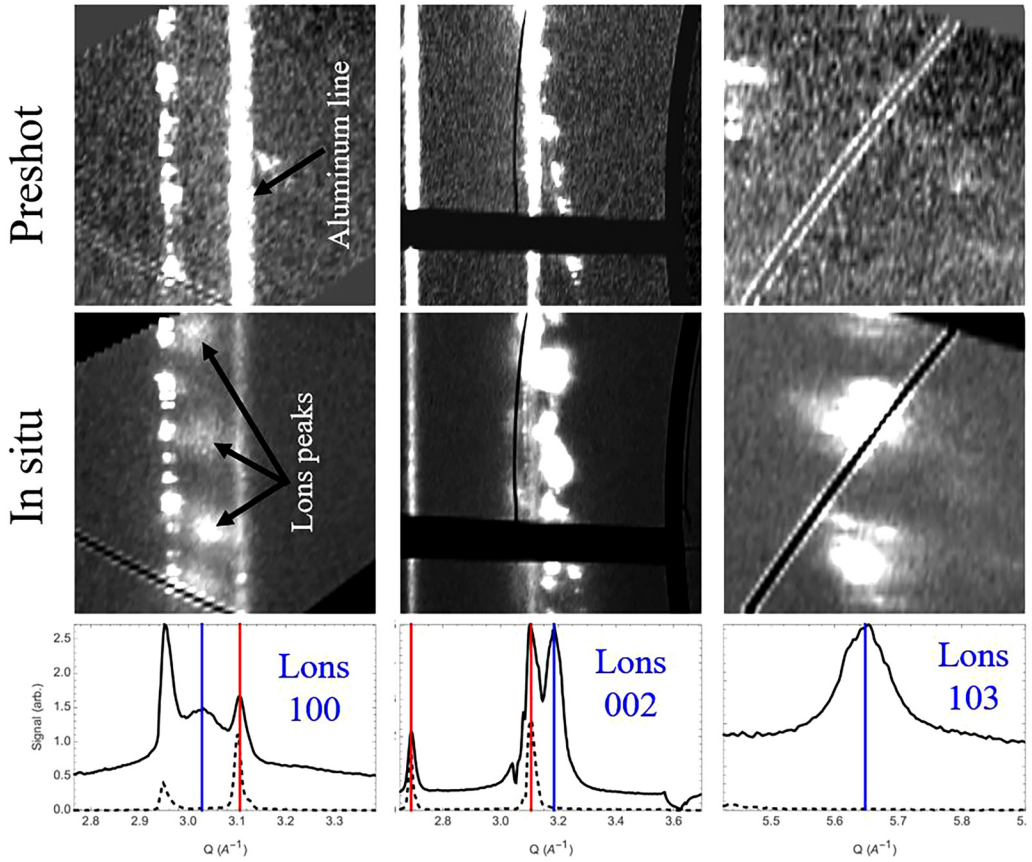


FIG. 5. 2D patterns in regions near the highlighted regions in Fig. 4 show diffraction lines identified as lonsdaleite and ambient aluminum before (pre-shot, top row) and during (*in situ* at 160 ps delay, middle row) compression. Corresponding integrated diffraction patterns over the azimuthal range of the 2D windows are shown at the bottom with fitted peak positions for lonsdaleite (blue vertical lines) and ambient aluminum (red vertical lines). Dashed lines are the integrated pre-shot patterns, and solid lines are the integrated *in situ* patterns, which show the appearance of peaks subsequent to compression. Due to the highly textured nature of the products, the integrated patterns only include data over a limited azimuthal range to aid in the identification of lonsdaleite peaks. The pinhole artifact gives a spurious peak near 2.95 A^{-1} in the left-most column (away from the lons 100 peak). A similar artifact cuts obliquely through the 2D window for the lons 002 peak but does not substantially contribute to the integrated signal, which is dominated by the compression-induced lons 002 peak.

identified by 100, 002, and 103 reflection peaks in the 2D patterns. Both the lonsdaleite and released graphite products are highly oriented, likely inheriting this preferred orientation from the initial highly oriented graphite. Unlike conventional, long time scale compression, here, crystallite products likely do not have sufficient time to reorient or undergo large plastic deformation. From estimates of the shock wave arrival time in HOPG, the phase transition occurred within tens of ps subsequent to compression, consistent with the time scale suggested by some molecular dynamics (MD) simulations.[31] As a consequence of a very strong crystallite orientation, no reflections of HOPG or lonsdaleite were observable in the Q range from ~3.3 to ~5.3 A^{-1} in any data. The fact that these reflections are not observed can be interpreted as a systematic absence. Therefore, we modeled a carbon phase that only shows reflections at the Q values of the two prominent spotty diffraction features at 3.0–3.1 and 5.6–5.7 A^{-1}. This structure can be derived by mapping the cell of lonsdaleite onto a hexagonal supercell cell with $\frac{1}{2}$ times the a- and b-axes and with C residing on site 4e (with possible orthorhombic distortion—see Sec. V). This site has only partial occupancy below ½ to avoid unphysical C–C distances and an occupancy ~0.4 reproduces the density of ordered lonsdaleite. Hence, this model phase is a disordered lonsdaleite structure. Taken together, the available data support formation of lonsdaleite, potentially with some level of structural disorder—see further comments in Sec. V.

To generally demonstrate the observation of lonsdaleite, Fig. 6 shows estimates of density from peak positions for two assumptions: (1) the lonsdaleite phase with the three observed peaks assigned to lonsdaleite 100, 002, and 103 reflections and (2) the graphite phase with peaks assigned to graphite 100, 101, and 112 reflections. Just subsequent to compression (at times between about 160 and 240 ps), for the lonsdaleite phase assumption, all three line

14 December 2023 08:14:40

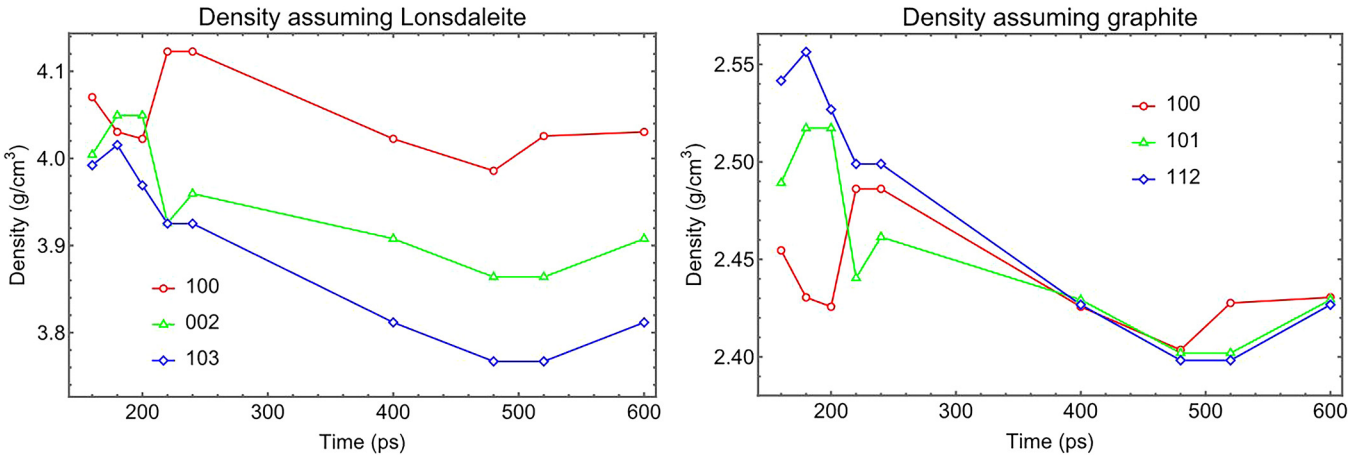


FIG. 6. Densities from peak shifts assuming the lonsdaleite phase (left) and the graphite phase (right).

positions give a consistent density of around 4 g/cm^3, which is also consistent with the pressure estimate of around 80 Gpa, given by impedance matching along the graphite Hugoniot (for compression by Al at 100 GPa). At later times (when the pressure is expected to release), the graphite phase assumption gives consistent line positions at substantially lower pressure. The earliest detection of lonsdaleite signal occurred between 140 and 160 ps delay after shock launch in the Al ablator, consistent with the arrival time estimated from hydrodynamics simulations, 160 ps. This suggests an upper bound for the phase transition time of 20 ps. This estimate is limited by a 20 ps interval between time delays, uncertainty in the shock arrival time from simulations, and a minimum amount of converted material to diffract enough signal to be observable.

We observe the back transformation to graphite within 300 ps after the release of the sample, when a distorted graphite peak correlated with the release of the sample is observed at around 6 A^{-1}. This effect is distinct from the appearance of lonsdaleite upon compression. In particular, the appearance of strong graphite peaks at high Q (>6 A^{-1}) occurs for all data, including the lowest pressure data at 2.5 mJ drive energy. Late time diffraction patterns exhibit a substantial growth of graphite peaks for Q values greater than about 6 A^{-1} subsequent to release but do not exhibit peaks in the range from ~3.2 to ~5.3 A^{-1}, suggesting that the sample remains highly oriented.

IV. CHARACTERIZATION OF THE CARBON PHASES PRESENT DURING SHOCK

Full frames with integrated patterns inset are shown in Fig. S1 in the supplementary material. The collected image frames include parasitic diffraction, evident as spotty fringes centered around a markedly different location than the primary beam that illuminates the sample, with one example labeled "artifact" in Fig. 1. Other artifacts in the integrated patterns result from a broad diffuse diffraction peak from incipient Bragg diffraction of the Si wafer, and gaps between the detector segments and enhanced signal at the borders of the detector segments generate negative offsets or cusps in the integrated pattern. All these features were excluded from integration of the diffraction signal by using the masking function of Dioptas.[39] At some locations in the detector plane, parasitic diffraction intersects sample diffraction. Also, all sample-related diffraction was observed at azimuthal angles where the signal was not compromised by parasitic diffraction. An additional artifact was noticed at the second step: at an elevated signal level, the response of some detector segments was different from the rest and resulted in broad features in the integrated patterns. These features in the integrated patterns do not correspond to any measurable signal in the actual frames and were suppressed by masking most or all of the affected detector segments. Fortunately, there was no sample-related diffraction signal that occurred only in these problematic detector segments. In Fig. S1 in the supplementary material, the masked regions appear black. Our analysis is based on (a) observation of the new peaks and (b) their disappearance upon shock release. Only graphite is observed upon release below ~80 GPa. Any other carbon phase that is formed during dynamic compression transforms back into graphite. Although Fig. 6 indicates that the compressed sample is more consistent with the lonsdaleite equation of state, a more detailed analysis also supports this conclusion. We now discuss the nature of shocked carbon material based on its diffraction signal.

Figure 4 compares pre-shot and *in situ* XRD patterns from the same run and sample. Carbon diffraction during HOPG compression exhibits pronounced broad Bragg reflections [marked by ellipses in Fig. 4 (*in situ*) and Fig. S1 in the supplementary material]. In addition, smooth Debye fringes with intensity modulation along the azimuthal angle are observed. The modulated intensity indicates the texture (that is: crystallite preferred orientation along more than one axis) of the grains that generate this signal. For the most pronounced fringe (near Qs of 3.03 and 3.2 A^{-1}), the diffraction angle matches that of the pronounced Bragg peaks. We examined the Debye fringes by integrating the diffraction images with the pronounced Bragg peaks masked: the

14 December 2023 08:14:40

powder statistics of this fraction of material allows for phase identification, as long as the effect of texture on the diffraction intensities is taken into account. We find that this fine-grained fraction is best fitted by lonsdaleite: The fringes at Q of 3.03 and 3.2 A^{-1} match lonsdaleite 100 and 002, and additional weak features at higher Q (5.65 A^{-1}) can be also explained as reflections of lonsdaleite. The observed c/a ratio is 1.65 (1) and the unit cell volume from this analysis corresponds to a density of 3.9 g/cm^3 consistent with Kraus *et al.* However, we note that some reflections of lonsdaleite such as 101 and 102 are not observed. The orientation-induced modification of diffraction intensities may account for a marked suppression of reflections within some ranges of the azimuthal angle but also implies a marked enhancement of intensity within complementary angular ranges. It is possible that these ranges are not probed by our limited diffraction aperture, but it also cannot be proven.

Therefore, we tested an alternative model that is based on the intense carbon reflections at Fig. 4 regions, labeled Lons 002 and Lons 103, and at 80.5° (see Fig. S1 in the supplementary material in the 220 and 260 ps frames). In addition, we assume that the absence of observable carbon diffraction signal between 3.2 $A^{-1} < Q < 5.6$ A^{-1} is not an accidental result of orientation, but intrinsic to the structure of compressed carbon. With this information, we are able to model a carbon structure that has observable reflections only at these angles through group-subgroup mapping from lonsdaleite. The mapping, cell dimensions, and fractional atomic coordinates are given in the supplementary material. The structure bears basic features of lonsdaleite through a tetrahedral network of C–C bonds with length 1.47 ± 0.05 A, while the multiplicity of its only, partially occupied site generates a number of potentially occupied positions every 1.5 A along the c-axis, which are equivalent to compressed graphitic sheets as proposed by Scandolo *et al.*[44] and Wang *et al.*[45] The intermediate states calculated by Scandolo *et al.*[44] and Wang *et al.*[45] are ordered, while the present model exhibits intrinsic lattice disorder with partially occupied sites.

We note that this model represents the features near 3.2 A^{-1} (Fig. 4 *in situ*, Fig. S1 in the supplementary material) as a single reflection, whereas (for instance) Fig. S1 in the supplementary material 220 ps shows that there are two distinct peaks near this Q. This can be explained by a mixture of ordered lonsdaleite and disordered lonsdaleite. However, it is more plausible that the disordered model structure represents a limiting state of atomic scale disorder of lonsdaleite, whereas the real material in the experiment is intermediate between this state and fully ordered lonsdaleite. In particular, an intermediate structural state explains (a) the absence of diffraction intensity between 3.2 $A^{-1} < Q < 5.6$ A^{-1} and (b) the observation of two distinct peaks at near 3.2 A^{-1} that match lonsdaleite 100 and 002. With the available data, a more accurate modeling of this disorder is not possible.

V. DISCUSSION

We note that for the peak conditions studied here (~80 GPa), the carbon phase diagram would indicate cubic diamond formation, exclusively. However, recent *in situ* XRD experiments have indicated a preponderance of hexagonal diamond formation under dynamic high pressure loading, with no observable cubic diamond.[11] Supporting density functional theory (DFT) calculations for a diffusionless phase transformation confirm that the kinetic barrier for hexagonal diamond formation is slightly lower than that for cubic diamond (1.99 vs 2.08 eV), though this could be within the error limits of those computations. These results hold true for both hydrostatic and non-hydrostatic conditions.[46] In contrast, the DFT calculations from Stavrou *et al.*[11] yield a small favorable relative enthalpy for a cubic diamond at high pressure (e.g., ~0.1 eV lower than that of hex diamond at 40 GPa). This indicates the possibility of both phases co-existing under extreme conditions, with possible kinetic trapping of the hexagonal phase. Previous studies on the high pressure phases of carbon make it likely that the energetic barrier for interconversion of hex to cubic is extremely large ($\gg k_BT$).[47] This phase co-existence is confirmed by MD simulations of shock-compressed graphite using a multi-phase carbon model which shows simultaneous regions of both hexagonal and cubic diamonds at peak shock conditions.[48]

Quantum MD simulations of graphite under a range of ultrafast strain rates have indicated that strongly overdriven loading stresses (e.g., in excess of 100 GPa) were required to induce phase transition to the cubic diamond on picosecond timescales (similar to the time resolution of the experimental measurements discussed here).[49] This study also yielded an extensive presence of defective regions which included both local disorder and the hexagonal diamond. This would indicate that high stresses likely reduce the energetic barrier for phase interconversion closer to k_BT. A possible mechanism for this process could involve a layered structure,[31] where the formation of hexagonal or cubic diamond sub-regions depends on the instantaneous local stacking of the graphite layers. Indeed, the low kinetic barrier for the sliding of graphite basal planes (approximately, 0.06 eV) would indicate that intermediate stacking states (e.g., ABCABC vs ABAB) would be thermally activated under ambient (pre-shock) conditions. We have somewhat explored this hypothesis by performing XRD predictions of layered diamond structures under slight shear strain to mimic this scenario (structures available on request). However, these intermediate states are of low symmetry and yield a slew of additional XRD peaks that were not present in any of our experimental measurements. Previous calculations have indicated that these high pressure layered states have extremely short lifetimes (e.g., less than 1 ps),[31] and hence, could be difficult to observe with the timescales probed here.

We note that the direct transformation of graphite to diamond appears to occur along different pathways where pressure, temperature, presence of additional chemical agents or catalysts, and the time scale are important. Martensitic transformation pathways are, in principle, favored during dynamic compression[50] in compression and seem inevitable in experiments where the peak shock compression is restricted to the ps time scale (such as in the present study). The absence or presence of lonsdaleite as an independent crystalline phase can constrain the possible martensitic pathways.[51–53] The product lonsdaleite exhibits strong, nearly single crystal texturing, i.e., intense, spotty peaks over a narrow azimuthal range. Integrated diffraction patterns over the entire detected azimuthal range were difficult to interpret since signals due to compressed aluminum and artifacts could not be distinguished from product

14 December 2023 08:14:40

lonsdaleite. Yet, as shown in Fig. 5, highly textured lonsdaleite peaks were identified in all the 2D patterns that interrogated compressed HOPG. Generally, we expect that the interpretation of diffraction data from materials under non-equilibrium, non-hydrostatic stress will require a more sophisticated analysis of the 2D patterns. Further orientational analyses of these data are included in the supplementary material.

The direct transition from graphite to diamond(−3C) or its hexagonal polytype lonsdaleite (diamond-2H) under static pressure, but in the absence of catalysts or other chemical agents, has been suggested to be diffusionless.[32] This is consistent with group-theoretical considerations of the transformation pathways.[51] Atomistic simulations of diamond nucleation in graphite suggest that the growth of cubic diamond is favorable over the formation of lonsdaleite, which only forms as a domain within the diamond.[52] Observations in natural impact-related diamonds[13] support these simulations, but this prediction is not supported by some other static and dynamic experiments[10,54] and other simulations.[53]

VI. CONCLUSION

It is interesting to note the strong role of kinetics in determining the shock pressure needed to drive the diamond or lonsdaleite phase transition at different time scales. For longer scale (many nanoseconds) experiments, 50 GPa is sufficient,[10,11] while at picosecond time scales, the needed pressure appears to be much higher. Here, we find that over the very short compression time and length scales of this experiment, the diffraction peaks in compressed HOPG are sufficiently narrow to identify product states, in this case, cubic and predominantly hexagonal diamond. Furthermore, although it is possible to compare temperatures and pressures obtained from quasi-equilibrium experiments and calculations,[10,49] we note that the states accessed in this experiment are explicitly non-equilibrium (lonsdaleite is not a thermodynamically stable phase in the equilibrium phase diagram of carbon), and, thus, estimates of pressure and temperature must be considered with care. Future works must consider an expanded range of non-hydrostatic stress states, just as a full range of 2D diffraction patterns must be employed.

Generally, these results are consistent with the observation of lonsdaleite in impact (i.e., shock) compressed graphite. These data further suggest that the formation of lonsdaleite is kinetically favored (over cubic diamond) under rapid compression. Consistent with speculation in an early shock compression work[14] and more recent static studies of diamonds from impact events,[16,17] these experiments suggest that the formation mechanism is martensitic (i.e., does not require long time scale diffusion), and at very early times, the orientation of the lonsdaleite product is correlated with the initial graphite orientation. This work connects inferences based on the structure of the diamond product to a dynamic experiment at a near *ab initio* scale.

SUPPLEMENTAL MATERIAL

See supplementary material for the analysis and fitting of diffraction patterns integrated over the entire azimuthal range, a detailed discussion of fits and implications for texture and disorder, and parameterization of the HOPG equation of state.

ACKNOWLEDGMENTS

Thanks, Evan, for your friendship and insight. You will be greatly missed.

Lawrence Livermore National Laboratory is operated by Lawrence Livermore National Security, LLC, for the U.S. Department of Energy, National Nuclear Security Administration under Contract No. DE-AC52-07NA27344. We acknowledge J. M. Zaug and J. C. Crowhurst for helpful discussions and planning support. We gratefully acknowledge the LLNL LDRD program for funding support of this project under No. 16-ERD-037 and DTRA Basic Science Grant No. HDTRA1-16-1-0020. This work was partially sponsored by the Department of the Defense, Defense Threat Reduction Agency under the Materials Science in Extreme Environments University Research Alliance, No. HDTRA1-20-2-0001. The content of the information does not necessarily reflect the position or the policy of the federal government, and no official endorsement should be inferred. A.E.G. acknowledges LANL LDRD Reines support. A.F.G., N.H., and S.L. acknowledge the support of the Army Research Office (Grant Nos. 56122-CH-H and 71650-CH W911NF-19-2-0172), Carnegie Institution of Washington, and NSF. V.P. acknowledges support from the National Science Foundation-Earth Sciences (No. EAR-1634415) and the Department of Energy-GeoSciences (No. DEFG02-94ER14466). Use of the Linac Coherent Light Source (LCLS), SLAC National Accelerator Laboratory, is supported by the U.S. Department of Energy Office of Science, Office of Basic Energy Sciences under Contract No. DE-AC02-76SF00515. The MEC instrument is supported by the U.S. Department of Energy, Office of Science, Office of Fusion Energy Sciences under Contract No. SF00515.

AUTHOR DECLARATIONS

Conflict of Interest

The authors have no conflicts to disclose.

Author Contributions

Michael R. Armstrong: Conceptualization (lead); Data curation (equal); Formal analysis (lead); Funding acquisition (supporting); Investigation (equal); Methodology (lead); Project administration (lead); Resources (equal); Supervision (equal); Validation (equal); Visualization (lead); Writing – original draft (lead); Writing – review and editing (equal). **Harry B. Radousky:** Conceptualization (equal); Data curation (equal); Formal analysis (supporting); Funding acquisition (lead); Investigation (equal); Project administration (equal); Resources (equal); Writing – original draft (supporting); Writing – review and editing (equal). **Ryan A. Austin:** Formal analysis (equal); Software (lead); Validation (equal); Visualization (equal); Writing – original draft (supporting); Writing – review and editing (supporting). **Oliver Tschauner:** Formal analysis (lead); Methodology (lead); Software (equal); Visualization (supporting); Writing – original draft (equal); Writing – review and editing (equal). **Shaughnessy Brown:** Data curation (supporting); Investigation (supporting). **Gowoon Cheon:** Software (supporting). **Nir Goldman:** Conceptualization (equal); Software (supporting). **Eduardo Granados:** Investigation

14 December 2023 08:14:40

(supporting); Methodology (supporting); Supervision (supporting). **Paulius Grivickas:** Investigation (supporting); Resources (equal). **Nicholas Holtgrewe:** Investigation (supporting). **Matthew P. Kroonblawd:** Software (supporting). **Hae Ja Lee:** Conceptualization (supporting); Data curation (equal); Investigation (equal); Project administration (equal); Supervision (equal). **Sergey Lobanov:** Investigation (supporting). **Bob Nagler:** Investigation (supporting); Methodology (supporting); Supervision (supporting). **Inhyuk Nam:** Investigation (supporting). **Vitali Prakapenka:** Formal analysis (equal); Investigation (supporting); Writing – review and editing (supporting). **Clemens Prescher:** Formal analysis (equal); Investigation (equal); Software (lead); Writing – review and editing (supporting). **Evan J. Reed:** Conceptualization (supporting); Software (equal). **Elissaios Stavrou:** Formal analysis (equal); Investigation (supporting); Writing – review and editing (supporting). **Peter Walter:** Investigation (supporting). **Alexander F. Goncharov:** Conceptualization (equal); Formal analysis (equal); Funding acquisition (supporting); Investigation (equal); Project administration (supporting); Resources (equal); Supervision (equal); Writing – original draft (equal); Writing – review and editing (equal). **Jonathan L. Belof:** Funding acquisition (lead); Investigation (supporting); Supervision (equal); Writing – original draft (supporting); Writing – review and editing (supporting).

DATA AVAILABILITY

The data that support the findings of this study are available from the corresponding authors upon reasonable request.

REFERENCES

[1]V. Georgakilas, J. A. Perman, J. Tucek, and R. Zboril, Chem. Rev. **115**, 4744 (2015).
[2]V. N. Mochalin, O. Shenderova, D. Ho, and Y. Gogotsi, Nat. Nanotechnol. **7**, 11 (2012).
[3]N. Nunn, M. Torelli, G. McGuire, and O. Shenderova, Curr. Opin. Solid State Mater. Sci. **21**, 1 (2017).
[4]S. S. Batsanov, S. M. Gavrilkin, A. S. Batsanov, K. B. Poyarkov, I. I. Kulakova, D. W. Johnson, and B. G. Mendis, J. Mater. Chem. **22**, 11166 (2012).
[5]D. J. Kennett, J. P. Kennett, A. West, G. J. West, T. E. Bunch, B. J. Culleton, J. M. Erlandson, S. S. Que Hee, J. R. Johnson, C. Mercer, F. Shen, M. Sellers, T. W. Stafford, A. Stich, J. C. Weaver, J. H. Wittke, and W. S. Wolbach, Proc. Natl. Acad. Sci. U.S.A. **106**, 12623 (2009).
[6]C. S. Kennedy and G. C. Kennedy, J. Geophys. Res. **81**, 2467 (1976).
[7]X. Wang, S. Scandolo, and R. Car, Phys. Rev. Lett. **95**, 185701 (2005).
[8]D. Erskine and W. Nellis, Nature **349**, 317 (1991).
[9]S. J. Turneaure, S. M. Sharma, T. J. Volz, J. M. Winey, and Y. M. Gupta, Sci. Adv. **3**, eaao3561 (2017).
[10]D. Kraus, A. Ravasio, M. Gauthier, D. O. Gericke, J. Vorberger, S. Frydrych, J. Helfrich, L. B. Fletcher, G. Schaumann, B. Nagler, B. Barbrel, B. Bachmann, E. J. Gamboa, S. Göde, E. Granados, G. Gregori, H. J. Lee, P. Neumayer, W. Schumaker, T. Döppner, R. W. Falcone, S. H. Glenzer, and M. Roth, Nat. Commun. **7**, 10970 (2016).
[11]E. Stavrou, M. Bagge-Hansen, J. A. Hammons, M. H. Nielsen, B. A. Steele, P. Xiao, M. P. Kroonblawd, M. D. Nelms, W. L. Shaw, W. Bassett, S. Bastea, L. M. Lauderbach, R. L. Hodgin, N. A. Perez-Marty, S. Singh, P. Das, Y. Li, A. Schuman, N. Sinclair, K. Fezzaa, A. Deriy, L. D. Leininger, and T. M. Willey, Phys. Rev. B **102**, 104116 (2020).
[12]C. Frondel and U. B. Marvin, Nature **214**, 587 (1967).
[13]P. Németh, L. A. J. Garvie, T. Aoki, N. Dubrovinskaia, L. Dubrovinsky, and P. R. Buseck, Nat. Commun. **5**, 5447 (2014).
[14]D. J. Erskine and W. J. Nellis, J. Appl. Phys. **71**, 4882 (1992).
[15]T. J. Volz and Y. M. Gupta, Phys. Rev. B **103**, L100101 (2021).
[16]F. Nestola, C. A. Goodrich, M. Morana, A. Barbaro, R. S. Jakubek, O. Christ, F. E. Brenker, M. C. Domeneghetti, M. C. Dalconi, M. Alvaro, A. M. Fioretti, K. D. Litasov, M. D. Fries, M. Leoni, N. P. M. Casati, P. Jenniskens, and M. H. Shaddad, Proc. Natl. Acad. Sci. U.S.A. **117**, 25310 (2020).
[17]Y. Nakamuta and S. Toh, Am. Mineral. **98**, 574 (2013).
[18]J. C. Crowhurst, M. R. Armstrong, K. B. Knight, J. M. Zaug, and E. M. Behymer, Phys. Rev. Lett. **107**, 144302 (2011).
[19]V. H. Whitley, S. D. McGrane, D. E. Eakins, C. A. Bolme, D. S. Moore, and J. F. Bingert, J. Appl. Phys. **109**, 013505 (2011).
[20]B. J. Demaske, V. V. Zhakhovsky, N. A. Inogamov, and I. I. Oleynik, Phys. Rev. B **87**, 054109 (2013).
[21]D. Milathianaki, S. Boutet, G. J. Williams, A. Higginbotham, D. Ratner, A. E. Gleason, M. Messerschmidt, M. M. Seibert, D. C. Swift, P. Hering, J. Robinson, W. E. White, and J. S. Wark, Science **342**, 220 (2013).
[22]V. V. Zhakhovsky, M. M. Budzevich, N. A. Inogamov, I. I. Oleynik, and C. T. White, Phys. Rev. Lett. **107**, 135502 (2011).
[23]M. R. Armstrong, J. M. Zaug, N. Goldman, I.-F. W. Kuo, J. C. Crowhurst, W. M. Howard, J. A. Carter, M. Kashgarian, J. M. Chesser, T. W. Barbee, Jr., and S. Bastea, J. Phys. Chem. A **117**, 13051 (2013).
[24]S. D. McGrane, D. S. Moore, and D. J. Funk, J. Phys. Chem. A **108**, 9342 (2004).
[25]A. Vailionis, E. G. Gamaly, V. Mizeikis, W. Yang, A. V. Rode, and S. Juodkazis, Nat. Commun. **2**, 1 (2011).
[26]M. R. Armstrong, J. C. Crowhurst, J. M. Zaug, S. Bastea, and A. F. Goncharov, Appl. Phys. Lett. **105**, 021904 (2014).
[27]S. I. Ashitkov, M. B. Agranat, G. I. Kanel', P. S. Komarov, and V. E. Fortov, JETP Lett. **92**, 516 (2010).
[28]J. C. Crowhurst, B. W. Reed, M. R. Armstrong, H. B. Radousky, J. A. Carter, D. C. Swift, J. M. Zaug, R. W. Minich, N. E. Teslich, and M. Kumar, J. Appl. Phys. **115**, 113506 (2014).
[29]J. J. Gilman, Science **274**, 65 (1996).
[30]J. J. Gilman, Philos. Mag. B **71**, 1057 (1995).
[31]C. J. Mundy, A. Curioni, N. Goldman, I.-F. Will Kuo, E. J. Reed, L. E. Fried, and M. Ianuzzi, J. Chem. Phys. **128**, 184701 (2008).
[32]A. V. Kurdyumov, V. F. Britun, V. V. Yarosh, A. I. Danilenko, and V. B. Zelyavskii, J. Superhard Mater. **34**, 19 (2012).
[33]D. Kraus, A. Otten, A. Frank, V. Bagnoud, A. Blažević, D. O. Gericke, G. Gregori, A. Ortner, G. Schaumann, D. Schumacher, J. Vorberger, F. Wagner, K. Wünsch, and M. Roth, High Energy Density Phys. **8**, 46 (2012).
[34]D. Kraus, J. Vorberger, D. O. Gericke, V. Bagnoud, A. Blažević, W. Cayzac, A. Frank, G. Gregori, A. Ortner, A. Otten, F. Roth, G. Schaumann, D. Schumacher, K. Siegenthaler, F. Wagner, K. Wünsch, and M. Roth, Phys. Rev. Lett. **111**, 255501 (2013).
[35]M. R. Armstrong, H. B. Radousky, R. A. Austin, E. Stavrou, H. Zong, G. J. Ackland, S. Brown, J. C. Crowhurst, A. E. Gleason, E. Granados, P. Grivickas, N. Holtgrewe, H. J. Lee, T. T. Li, S. Lobanov, J. T. McKeown, B. Nagler, I. Nam, A. J. Nelson, V. Prakapenka, C. Prescher, J. D. Roehling, N. E. Teslich, P. Walter, A. F. Goncharov, and J. L. Belof, J. Mater. JOM **73**, 2185 (2021).
[36]H. B. Radousky, M. R. Armstrong, R. A. Austin, E. Stavrou, S. Brown, A. A. Chernov, A. E. Gleason, E. Granados, P. Grivickas, N. Holtgrewe, H. J. Lee, S. S. Lobanov, B. Nagler, I. Nam, V. Prakapenka, C. Prescher, P. Walter, A. F. Goncharov, and J. L. Belof, Phys. Rev. Res. **2**, 013192 (2020).
[37]H. B. Radousky, M. R. Armstrong, and N. Goldman, J. Appl. Phys. **129**, 040901 (2021).
[38]I. G. Grigorieva and A. A. Antonov, X-Ray Spectrom. **32**, 64 (2003).
[39]C. Prescher and V. B. Prakapenka, High Pressure Res. **35**, 223 (2015).
[40]W. Kraus and G. Nolze, J. Appl. Crystallogr. **29**, 301 (1996).

14 December 2023 08:14:40

[41]J. Colvin and J. Larsen, *Extreme Physics: Properties and Behavior of Matter at Extreme Conditions* (Cambridge Core, 2013).
[42]D. J. Steinberg, *Equation of State and Strength Properties of Selected Materials* (Lawrence Livermore National Laboratory, Livermore, CA, 1996).
[43]*LASL Shock Hugoniot Data*, edited by S. P. Marsh (University of California Press, Berkeley, CA, 1980).
[44]S. Scandolo, M. Bernasconi, G. L. Chiarotti, P. Focher, and E. Tosatti, Phys. Rev. Lett. **74**, 4015 (1995).
[45]J.-T. Wang, C. Chen, and Y. Kawazoe, Phys. Rev. B **85**, 033410 (2012).
[46]P. Xiao and G. Henkelman, J. Chem. Phys. **137**, 101101 (2012).
[47]J. Sun, D. D. Klug, and R. Martoňák, J. Chem. Phys. **130**, 194512 (2009).
[48]N. Pineau, J. Phys. Chem. C **117**, 12778 (2013).
[49]M. P. Kroonblawd and N. Goldman, Phys. Rev. B **97**, 184106 (2018).
[50]W. J. Nellis, A. C. Mitchell, and A. K. McMahan, J. Appl. Phys. **90**, 696 (2001).
[51]V. P. Dmitriev, S. B. Rochal, Y. M. Gufan, and P. Tolédano, Phys. Rev. Lett. **62**, 2495 (1989).
[52]S. Zhu, X. Yan, J. Liu, A. R. Oganov, and Q. Zhu, Matter **3**, 864 (2020).
[53]H. Xie, F. Yin, T. Yu, J.-T. Wang, and C. Liang, Sci. Rep. **4**, 5930 (2015).
[54]V. F. Britun, A. V. Kurdyumov, and I. A. Petrusha, Powder Metall. Met. Ceram. **43**, 87 (2004).

14 December 2023 08:14:40